Electronic Structure, Ion Diffusion and Cation Doping in the $Na_4VO(PO_4)_2$ Compound as a Cathode Material for Na-ion Batteries

Pablo A. Aparicio[a,*] and Nora H. de Leeuw[a,b*]

[a] *School of Chemistry, Cardiff University, Main Building Park Place, Cardiff CF10 3AT, United Kingdom*

[b] *School of Chemistry, University of Leeds, Leeds LS2 9JT, United Kingdom*

Email:

*apariciosanchezp@cardiff.ac.uk

*n.h.deleeuw@leeds.ac.uk

Abstract

Sodium-ion batteries are considered one of the most promising alternatives to lithium-ion batteries owing to the low cost and wide abundance of sodium. Phosphate compounds are promising materials for sodium-ion batteries because of their high structural stability, energy densities and capacities. Vanadium phosphates have shown high energy densities, but their sodium-ion diffusion and cation doping properties are not fully rationalized. In this work, we combine density functional theory calculations and molecular dynamics simulations to study the electronic structure, ion diffusion and cation doping properties of the $Na_4VO(PO_4)_2$ compound. The calculated Na-ion activation energy of this compound is 0.49 eV, which is typical for Na-based cathode materials, and the simulations predict a Na-ion diffusion coefficient of 5.1×10^{-11} cm^2 s^{-1}. The cell voltage trends show a voltage of 3.3 V *vs.* Na/Na^+. Partial substitution of vanadium atoms by other metals (Al^{3+}, Co^{2+}, Fe^{3+}, Mn^{4+}, Ni^{2+} or Ti^{4+}) increases the cell voltage up to 1.1 V *vs.* Na/Na^+. These new insights will help us to understand the ion transport and electrochemical behaviour of potential phosphate cathode materials for sodium-ion batteries.

1. Introduction

The development of large-scale energy storage systems (ESSs) has become one of the most important research areas in recent years.[1–3] Among several ESSs, lithium-ion batteries (LIBs) have been considered one of the most promising systems based on their high energy densities.[4,5] However, issues remain with LIBs as grid-scale ESSs, e.g. their increasing cost owing to limited global lithium resources to satisfy the high demand.[6] As such, sodium-ion systems are a less expensive and more abundant alternative for lithium-based ESSs and rechargeable batteries based on sodium have been studied in some depth in the quest to obtain cheaper and more sustainable ESSs.[7–11] Sodium-ion batteries (NIBs) are of particular interest for grid-scale ESSs for intermittent renewable energy.[12–15]

Considerable effort has been expended to obtain new sodium materials for NIBs that show high reversible capacity, rapid ion insertion-extraction and cycling stability.[16,17] Different compounds, such as metal oxides, polyanionic compounds and Prussian blue analogues, have demonstrated large sodium storage abilities for NIB applications. In particular, vanadium phosphate compounds such as $NaVOPO_4$, $NaVPO_4F$, $Na_3V_2(PO_4)_3$ and $Na_3V_2(PO_4)_2F_3$, show good electrochemical performance[18–21] and are promising cathode materials owing to their versatile structure, high stability, long-term cycling and low volumetric expansion during sodium insertion/extraction.

Recently, Kim and co-workers have explored the high-power cathode material $Na_4VO(PO_4)_2$ for NIB applications,[22] which has shown high redox potential and has an open framework for fast Na-ion diffusion. Deriouche et al. also examined the electrochemical properties of the $Na_4VO(PO_4)_2$ compound, demonstrating its high ionic conductivity and stability up to 700º C.[23] Previous works have demonstrated that cathode materials for NIBs with the V^{4+}/V^{5+} redox couple and the inductive effect of phosphorous ions, such as $Na_3V_2(PO_4)_3$ and $Na_3V_2(PO_4)_2F$, exhibit high operation voltages.[20,21,24,25]

In this study, we have investigated for the first time the electronic structure, ion diffusion and cation doping properties of the $Na_4VO(PO_4)_2$ compound by employing an effective combination of ab initio calculations and classical molecular dynamics simulation. We were able to reproduce the experimental structural parameters, before predicting the Na-ion diffusion mechanisms and voltage trends as a result of metal doping, where the doped structures show

an increase in the cell voltage of up to 1.1 V *vs.* Na/Na^+. From the molecular dynamic simulations, we have computed an activation energy of 0.49 eV for sodium diffusion. As such,

this material has a high Na-ion diffusion coefficient and low activation energy for Na-ion migration, making it a promising cathode material for NIBs.

2. Methods

DFT calculations were performed using the Vienna Ab Initio Simulation Package (VASP).[26–29] We used Projector-Augmented Wave (PAW) pseudopotentials[30,31] and the Perdew-Burke-Ernzerhof exchange correlation functional revised for solids (PBEsol),[32] setting the kinetic energy cut-off at 520 eV. A k-point grid of 5 × 5 × 5 was used to converge the forces and energies of the bulk material. The DFT+U methodology was applied to account for the d orbitals of the metal atoms, with effective Hubbard values of U_{eff} = U - J = 4.0, 3.3, 4.3, 3.9, 6.0 and 4.2 eV (J = 1 eV) for V, Co, Fe, Mn, Ni and Ti, respectively.[21,33,34] These values are consistent with previous studies of vanadium compounds as cathode materials.[21,33] A smaller value of U_{eff} has been used for vanadium previously, leading to underestimated redox potentials compared to experimental values. It was reported that a larger value of U_{eff} (4.0 eV) gives more reliable agreement with experimental observations. In addition, Van der Waals contributions via the DFT-D3 method of Grimme[35] were included, as these have been shown to influence cell voltage calculations in some polyanionic systems.[36]

Previous computational studies on different metal oxide cathode materials have shown that such methods are suitable to compute accurate cell voltage trends.[37] Furthermore, they have also been shown to successfully determine transport and defect properties in Li-ion batteries.[38–40] The cell voltage *vs.* Na/Na^+ of the V^{4+}/V^{5+} redox couples were calculated using the following equations:

$$V = E[Na_4VO(PO_4)_2] - E[Na_3VO(PO_4)_2] - \mu[Na] \quad (1)$$

where $E[Na_4VO(PO_4)_2]$ and $E[Na_3VO(PO_4)_2]$ are the total energies of the $Na_4VO(PO_4)_2$ and $Na_3VO(PO_4)_2$ compounds, respectively. All the compounds were geometry optimized to relax their structures and obtain the most stable configuration. The chemical potential of sodium, [Na], was calculated using metallic sodium, which is the standard practice for cell voltage calculations. The MD simulations were performed using the LAMMPS code[41,42] and the calculations were carried out on a large supercell made up of 7 × 7 × 7 unit cells, comprising 15974 atoms. The initial configuration of the supercell contained 10% Na vacancies, plus corresponding V^{5+} species, which were randomly distributed. Pre-equilibrium runs of 4 ps using a time step of 2 fs within an NPT ensemble (constant number of particles, constant pressure and constant temperature) were first used to obtain stable configurations. Simulation

runs were carried out using the NVT ensemble (constant number of particles, constant pressure and constant temperature) and a time step of 1 fs for long runs of 10 ns, at temperatures in the range of 300–1400 K. The interatomic potentials used in the MD calculations are listed in Table SI1.

The mean squared displacement (MSD) of the Na cations, $[r(t)]^2$, for the $Na_4VO(PO_4)_2$ compound was computed to derive the diffusion coefficient (D_{Na}) using the equation:

$$= (\quad)(\langle[0]\rangle \qquad (2)$$

where t is time and $\langle[r(t)]^2\rangle$ is the MSD. A plot of the MSD *vs.* time at 300 and 600 K for the $Na_4VO(PO_4)_2$ compound can be found in the Supporting Information as Figure SI1.

3. Results and discussion

3.1 Structural analysis

The crystal structure, polymorphism and properties of $Na_4VO(PO_4)_2$ were first studied by Panin et al.[43] The high temperature phase, , crystallizes in the *Ibam* space group, whereas the low temperature phase, , crystallizes in the *Pbca* space group. It was shown that a reversible phase transition occurs at low temperature (~473 K). More recently, Lee and co-workers have explored the application of the $Na_4VO(PO_4)_2$ compound as a cathode material for NIBs,[22] where it showed high power capability owing to the high Na content, the numerous possible Na diffusion paths, and the open framework structure.

The $Na_4VO(PO_4)_2$ compound has a similar structure to the high temperature modification of the $Na_4TiO(PO_4)_2$ compound. The crystal structure of the $Na_4VO(PO_4)_2$ compound is depicted in Figure 1a and consists of infinite VO_6 chains sharing common apical corners. The vanadium octahedra are linked by two PO_4 tetrahedra resulting in a zigzag chain (Figure 1b). The vanadium atoms are shifted from the equatorial plane of the octahedra towards one of the apical oxygen atoms, forming short and long V-O bonds (1.75 and 2.04 Å, respectively), whereas all equatorial V-O distances are similar (1.94-1.99 Å). This geometry shows the formation of the characteristic vanadyl bond; these bonds have the same orientation along the *b*-axis of the neighbouring chains, whereas they are oriented in an opposite way along the *a*-axis. The phosphate groups are slightly distorted, showing P-O distances in the range of 1.52-1.56 Å.

The sodium atoms are located in the interstices between the chains and exist in four different coordination arrangements (Figure 1c). The Na(1) atoms are coordinated to six oxygen atoms forming a distorted octahedron with Na-O distances ranging from 2.30 to 2.46 Å. The Na(2)

atoms can be considered in a bicapped tetrahedron instead of an octahedron, showing Na-O distances in the range 2.24-2.82 Å. The Na(3) atoms are located in a distorted tetrahedron and coordinate four oxygen atoms with Na-O distances ranging from 2.27 to 2.41 Å. Na(3) has three extra neighbouring oxygen atoms, although at a separation of more than 3Å. The Na(4) atoms are sited in the centre of a seven-atom polyhedron, which can be considered as a distorted trigonal antiprism and shows Na-O distances in the range 2.32-2.82 Å. A comparison of the experimental and computed cell parameters and averaged bond lengths can be found in Table **1** (the list with all the bond lengths is given in the Table SI2). The computed values are in good agreement with the experimental cell parameters and bond lengths.

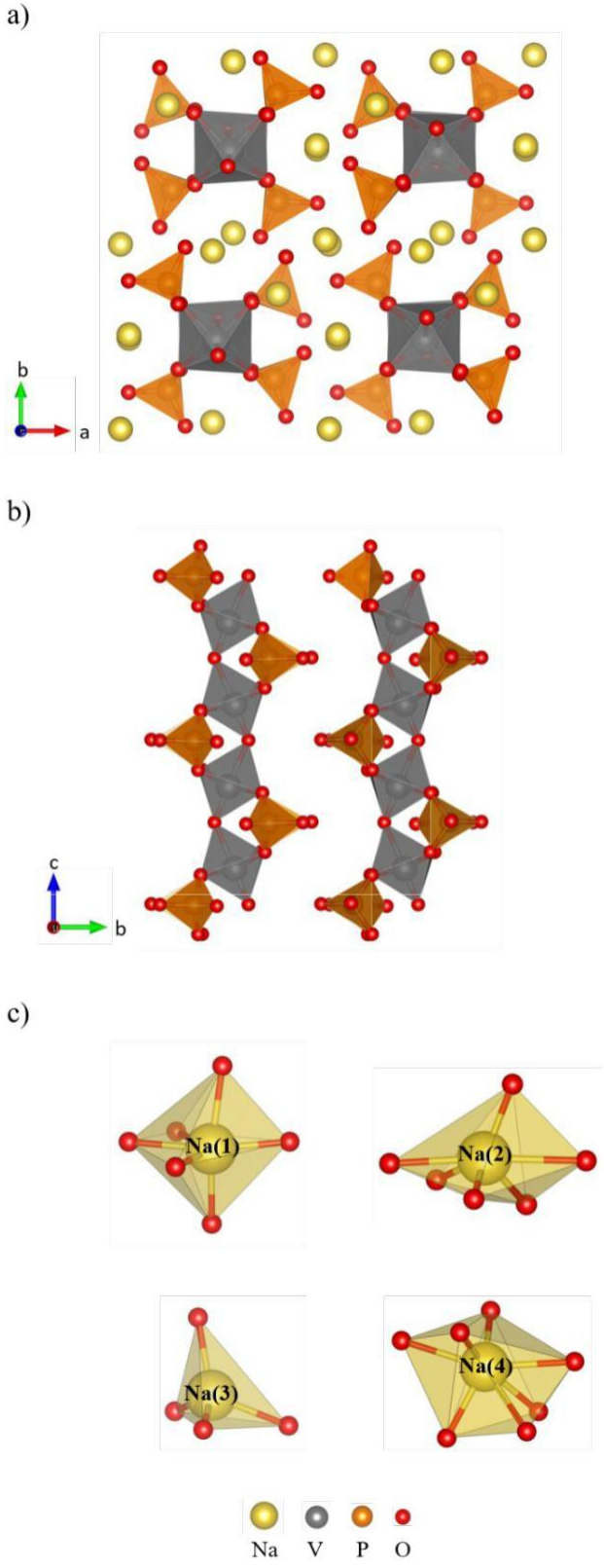

Figure 1. Polyhedral representation of (a) the $Na_4VO(PO_4)_2$ compound, (b) the vanadium chains connected with the phosphate groups, where sodium atoms have been omitted for clarity, and (c) the four different Na environments.

Table 1. Comparison of computed and experimental cell parameters and averaged bond lengths of $Na_4VO(PO_4)_2$ compound (in Å).

	$Na_4VO(PO_4)_2$	
	Comp.	Exp.[a]
a	15.976	15.949
b	14.458	14.462
c	6.921	6.999
V-O	1.944	1.928
P-O	1.548	1.545
Na(1)-O	2.390	2.411
Na(2)-O	2.443	2.444
Na(3)-O	2.346	2.373
Na(4)-O	2.548	2.572
Symmetry	Orthorhombic	
Space group	*Pbca*	

[a] Ref. [22].

Polyhedral representations of the doped materials $Na_4V_{1-x}M_xO(PO_4)_2$ (M = Al^{3+}, Co^{2+}, Fe^{3+}, Mn^{4+}, Ni^{2+} or Ti^{4+}, and x = 0.25 or 0.50) are shown in Figure 2. In these structures, the dopant atoms (M) have replaced either 25% or 50% of the V atoms. The crystal structures of the doped compounds consist of infinite MO_6 chains sharing apical corners, where the MO_6 octahedra are linked by two PO_4 tetrahedra resulting in a zigzag chain, as was also shown in Figure 1b. The M atoms form short and long M-O bonds in the apical axis, like the V atoms in both the pristine and doped materials. In the case of the Co-doped compound, the Co-O short and long bonds are 1.74 and 2.02 Å, respectively; which are very similar to the V-O distances (1.75 and 2.04 Å, respectively). However, the short M-O distances in Al-, Fe-, Mn-, Ni- and Ti-doped compounds are longer, ranging from 1.85 to 1.90 Å, although the long M-O distances retain values between 2.01 and 2.07 Å. The P-O and Na-O distances in all doped materials are comparable to those in the pristine material.

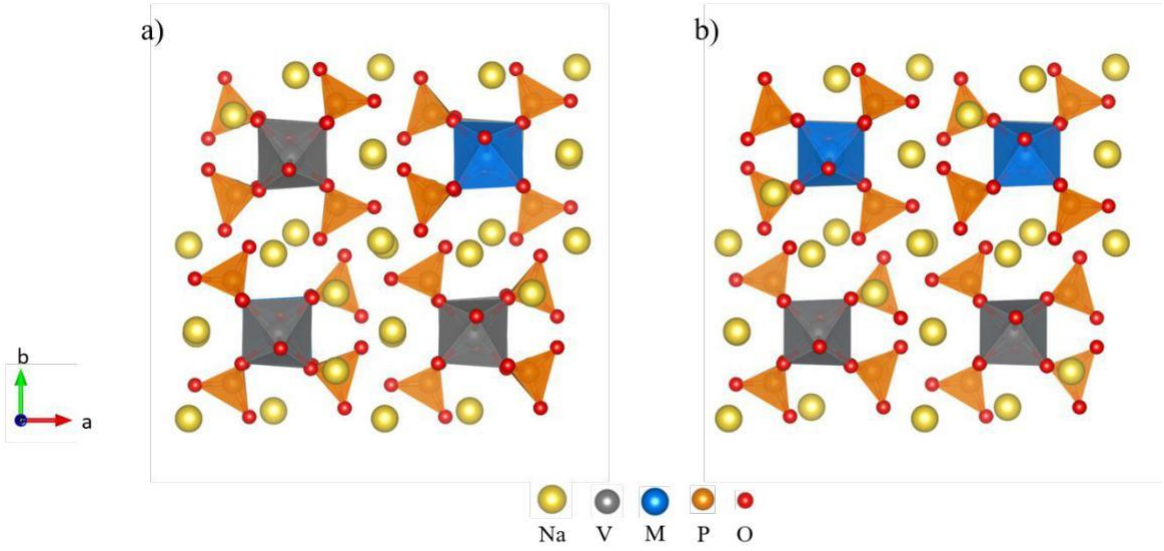

Figure 2. Polyhedral representation of the doped materials $Na_4V_{1-x}M_xO(PO_4)_2$, where M = Al^{3+}, Co^{2+}, Fe^{3+}, Mn^{4+}, Ni^{2+} or Ti^{4+}, and x = (a) 0.25 or (b) 0.50.

3.2 Cell voltage trend on cation doping

We have used the results from the DFT+U calculations to compute the cell voltages of the pure and doped $Na_4VO(PO_4)_2$ compounds. To carry out the calculations, Na ions were removed from the optimised structure and different vacancy positions were considered. The voltage was then calculated, using Equation 1, for the lowest energy configuration. The computed voltage of the $Na_4VO(PO_4)_2$ compound is 3.3 V *vs.* Na/Na^+, which is in good agreement with the experimental value of ~3.5 V *vs.* Na/Na^+.

We have also investigated how doping on the vanadium site affects the cell voltage of the $Na_4VO(PO_4)_2$ compound. The voltage trend of $Na_4V_{1-x}M_xO(PO_4)_2$ (M = Al^{3+}, Co^{2+}, Fe^{3+}, Mn^{4+}, Ni^{2+} or Ti^{4+}) *vs.* Na/Na^+ with varying x values (0, 0.25 or 0.50) is depicted in Figure 3. These particular substitutional cations have already been used as doping agents in different vanadium phosphate compounds, e.g. $NaVOPO_4$, $Li_3V_2(PO_4)_3$ and $Na_3V_2(PO_4)_3$.[44–52] The doped materials showed higher capacity than the pristine compounds and the addition of the cation dopants enhanced the electrochemical performance, the Li-ion and Na-ion diffusion, and the structural stabilisation.

The computed cell voltage values of some of the doped structures were above the voltage stability window for liquid Na-ion electrolytes (~3.5 V *vs.* Na/Na^+).[53] When x = 0.25, the Mn-and Ti-doped structures are the only compounds whose voltage is within the voltage stability window, whereas at x = 0.50, all the doped structures show computed voltages which are higher than the electrochemical window for liquid electrolytes. We also observed that in the doped materials, where the cation has an oxidation state different than 4+, some of the vanadium atoms are oxidised to V^{5+} to compensate the charge. To summarise, the Mn^{4+} and Ti^{4+} cations appear to be the most suitable dopants to increase the voltage of the $Na_4VO(PO_4)_2$ compound within the operating voltage window of liquid electrolytes.

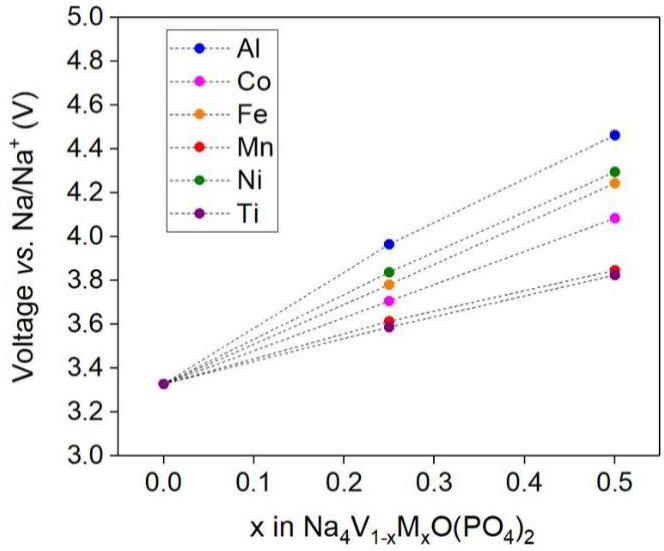

Figure 3. Cell voltage trend (*vs.* Na/Na^+) of the $Na_4V_{1-x}M_xO(PO_4)_2$ compound as function of dopant concentration (M = Al^{3+}, Co^{2+}, Fe^{3+}, Mn^{4+}, Ni^{2+} or Ti^{4+}) on the vanadium site.

3.3 Electronic analysis

The density of states (DOS) of the $Na_4VO(PO_4)_2$ compound is depicted in Figure 4. The reported Curie-Weiss temperature is below 2 K, indicating a very weak magnetic interaction

between the vanadium spins, which behave almost like free spins.[43]

configuration cannot be computed, so we compared the energy of the ferromagnetic and antiferromagnetic configurations. We found that the ferromagnetic solution, where all vanadium spins are parallel, is the more stable configuration of the two. The valence band of the DOS is described mainly by V 3d and O 2p electrons, whereas the conduction band is mainly made up of V 3d electrons and the P atoms make only a relatively small contribution to both valence and conduction bands. Below the Fermi level, from -0.3 to 0.0 eV, the total DOS shows a contribution from the V 3d and the O 2p states, which corresponds to the short V=O double bonds. The band gap of the studied compound is 1.8 eV, which is in good agreement with previous GGA+U results of different vanadium phosphate compounds.[54]

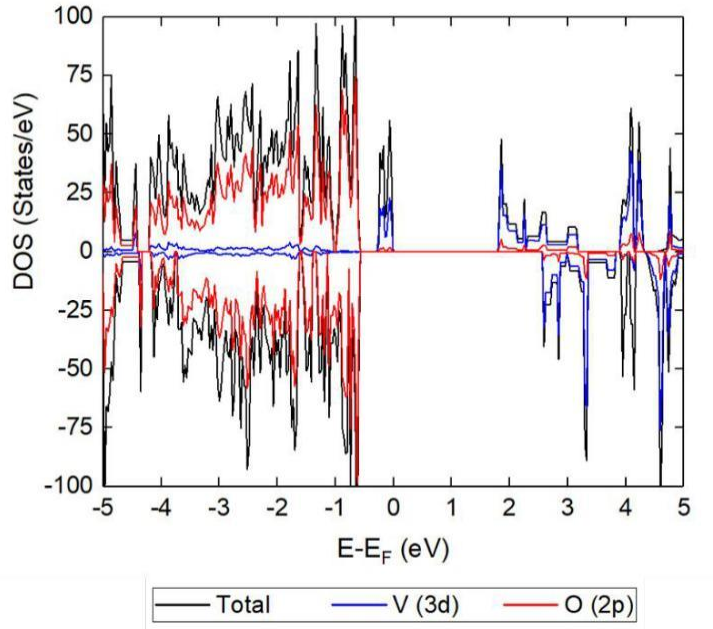

Figure 4. Density of States (DOS) of the $Na_4VO(PO_4)_2$ compound.

In general, the polyanionic compounds exhibit electronic properties of semiconductors or insulators. Metal-doping is a well-known strategy to change the electronic structure and improve ionic conductivity.[55–57] The electronic structure of the doped and pristine materials is very similar, with a small decrease of the band gap observed in all the doped compounds. Even though the decrease in the band gap is small, it can still facilitate electron conduction and thus accelerate the electron reaction kinetics. As a result, an improved electrochemical performance can be expected. The band gap reduction may be associated with the low electron affinity of the doped atoms compared to the V atom,[58] which causes an increase in the electronic conductivity.

3.3 Na-ion diffusion rates and pathways

MD simulations were performed over long timescales (10 ns) to examine long-range Na-ion transport. From the mean squared displacement (MSD) analysis, we observed that the diffusion takes place with equal probability in the three spatial directions. At 300 K, the diffusion coefficient (D_{Na}) of the $Na_4VO(PO_4)_2$ compound was calculated at 5.1×10^{-11} cm^2 s^{-1}. To the best of our knowledge, there are no experimental or computed values of this compound available in the literature for comparison. However, the computed D_{Na} is similar to those found in other vanadium phosphate cathode materials, e.g. $NaVOPO_4$ (10^{-11}-10^{-12} cm^2 s^{-1}),[59] and in other Na-ion cathode materials, such as Na_xCoO_2 (10^{-11} cm^2 s^{-1}),[60] Na_xMnO_2 (10^{-11} cm^2 s^{-1})[61] and Na_2CoSiO_4 (10^{-12} cm^2 s^{-1}).[62] Using the Nernst-Einstein equation we have converted the diffusion coefficient to conductivity which was found to be equal to 7.5×10^{-3} S cm^{-1}. This value obtained from our calculations is very similar to the experimental value of 10^{-4} S cm^{-1}. The MD calculations were performed at different temperatures between 300 and 1400 K, covering a larger range than only the typical NIB operating temperatures. The computed diffusion coefficients at different temperatures can be used to estimate activation energies from an Arrhenius plot (ln D_{Na} *vs.* 1/T), as shown in Figure 5.

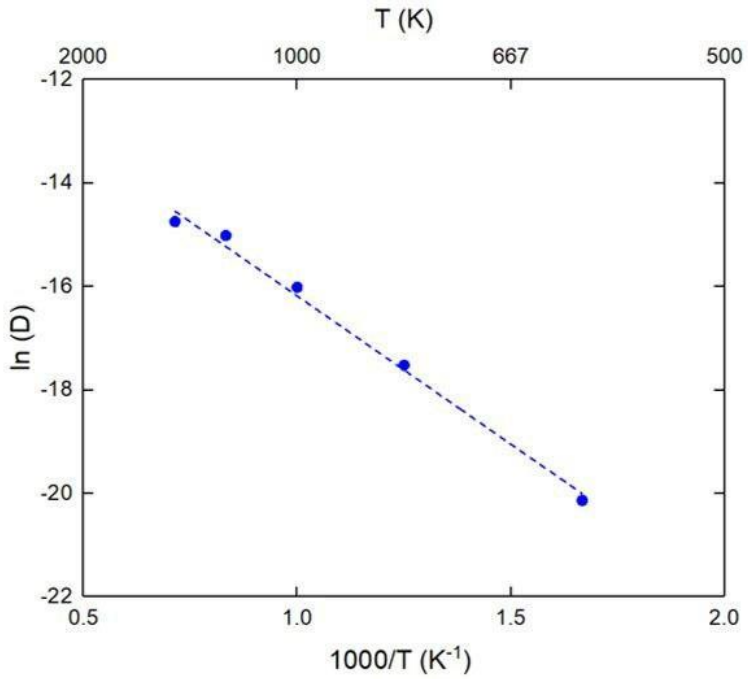

Figure 5. Arrhenius plot of Na-ion diffusion coefficients *vs.* temperature for the $Na_4VO(PO_4)_2$ compound.

The activation energy for the onset of diffusion of the sodium ion in the $Na_4VO(PO_4)_2$ compound was calculated at 0.49 eV, which is similar to the values of other vanadium phosphate compounds. Diffusion trajectories of Na ions are visualised in Figure 6 by plotting

accumulated Na-ion densities, indicating the most frequently crossed sites during the MD simulation. As derived from the MSD analysis, we observed from the Na densities that the diffusion takes place along 3D channels. These results confirm that Na ions are highly mobile

Figure 6. Na density plot from MD simulations at 700 K showing the Na diffusion pathways of the $Na_4VO(PO_4)_2$ compound. Na-ion density is plotted in yellow.

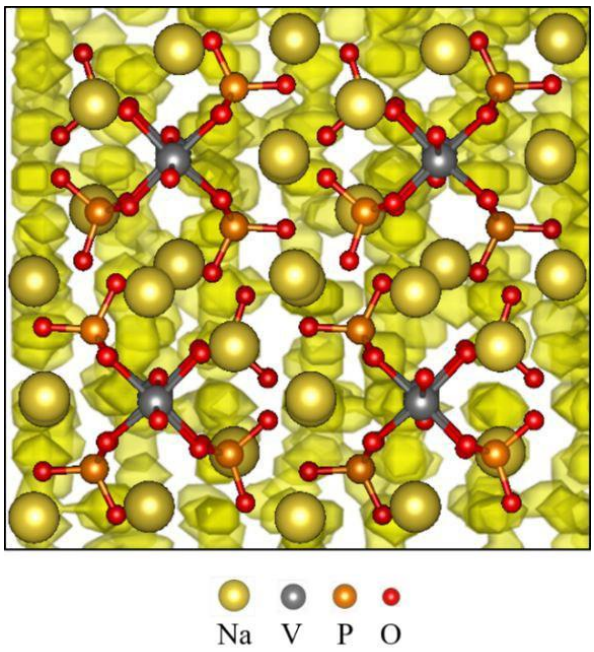

4. Conclusions

The sodium vanadyl phosphate $Na_4VO(PO_4)_2$ is one of the most promising cathode materials for sodium-ion batteries because of its good electrochemical performance. Here, we have studied the electronic structure, diffusion and cation doping properties of the $Na_4VO(PO_4)_2$ compound. Our work shows good reproduction of the observed experimental structure and it also reveals key atomistic insights into the ionic transport properties. From the MD simulations, we derived an Na ion activation energy of 0.49 eV and a diffusion coefficient at 300 K of $D_{Na} = 5.1 \times 10^{-11}$ cm^2 s^{-1}. Analysis of the migration pathways shows that the Na-ion diffusion in the $Na_4VO(PO_4)_2$ compound takes place along 3-dimensional channels. The DFT-computed cell voltage of 3.3 V *vs.* Na/Na$^+$ agrees well with the reported electrochemical data, whereas cation doping (Al^{3+}, Co^{2+}, Fe^{3+}, Mn^{4+}, Ni^{2+} and Ti^{4+}) at the vanadium site is predicted to increase the cell voltage. The Mn- and Ti-doped materials show an increase of the cell voltage within the electrochemical stability window of current liquid electrolytes.

Overall, the fundamental insights presented in this work will help us understand the ionic transport properties of phosphate cathode materials for sodium-ion batteries.

Author information

Corresponding authors:

apariciosanchezp@cardiff.ac.uk

deleeuwn@cardiff.ac.uk

Notes:

The authors declare no competing financial interest.

Acknowledgements

The authors acknowledge the Engineering and Physical Sciences Research Council (EPSRC) for financial support (Energy Materials Programme grant EP/K016288 and Platform grant EP/K009567). We also acknowledge ARCHER HPC facilities and the Materials Chemistry Consortium (EPSRC grant EP/L000202). All data created during this research are openly available from the Cardiff University Research Portal at http://dx.doi.org/xxxx.

References

1 K. C. Divya and J. Østergaard, *Electr. Power Syst. Res.*, 2009, **79**, 511–520.

2 B. Dunn, H. Kamath and J.-M. Tarascon, *Science (80-.).*, 2011, **334**, 928–935.

3 S. Hameer and J. L. van Niekerk, *Int. J. Energy Res.*, 2015, **39**, 1179–1195.

4 J.-M. Tarascon and M. Armand, *Nature*, 2001, **414**, 359–367.

5 M. Armand and J.-M. Tarascon, *Nature*, 2008, **451**, 652–657.

6 H. Vikström, S. Davidsson and M. Höök, *Appl. Energy*, 2013, **110**, 252–266.

7 S. W. Kim, D. H. Seo, X. Ma, G. Ceder and K. Kang, *Adv. Energy Mater.*, 2012, **2**, 710–721.

8 S. Y. Hong, Y. Kim, Y. Park, A. Choi, N.-S. Choi and K. T. Lee, *Energy Environ. Sci.*, 2013, **6**, 2067–2081.

9 H. Pan, Y.-S. Hu and L. Chen, *Energy Environ. Sci.*, 2013, **6**, 2338–2360.

10 N. Yabuuchi, K. Kubota, M. Dahbi and S. Komaba, *Chem. Rev.*, 2014, **114**, 11636–11682.

11 H. Kim, H. Kim, Z. Ding, M. H. Lee, K. Lim, G. Yoon and K. Kang, *Adv. Energy Mater.*, 2016, **6**, 1600943.

12 C. Fang, Y. Huang, W. Zhang, J. Han, Z. Deng, Y. Cao and H. Yang, *Adv. Energy* 3432–3448.
Mater., 2016, **6**, 1501727.

13 J.-Y. Hwang, S.-T. Myung and Y.-K. Sun, *Chem. Soc. Rev.*, 2017, **46**, 3529–3614.

14 D. Kundu, E. Talaie, V. Duffort and L. F. Nazar, *Angew. Chemie Int. Ed.*, 2015, **54**,

15 Q. Ni, Y. Bai, F. Wu and C. Wu, *Adv. Sci.*, 2017, **4**, 1600275.

16 N. Yabuuchi, K. Kubota, M. Dahbi and S. Komaba, *Chem. Rev.*, 2014, **114**, 11636–11682.

17 M. H. Han, E. Gonzalo, G. Singh and T. Rojo, *Energy Environ. Sci.*, 2015, **8**, 81–102.
19 J. Barker, M. Y. Saidi and J. L. Swoyer, *Electrochem. Solid-State Lett.*, 2003, **6**, A1–
18 J. Song, M. Xu, L. Wang and J. B. Goodenough, *Chem. Commun.*, 2013, **49**, 5280–5282.

21 R. A. Shakoor, D.-H. Seo, H. Kim, Y.-U. Park, J. Kim, S.-W. Kim, H. Gwon, S. Lee A4.

20 S. Y. Lim, H. Kim, R. A. Shakoor, Y. Jung and J. W. Choi, *J. Electrochem. Soc.*, 2012, **159**, A1393–A1397.

and K. Kang, *J. Mater. Chem.*, 2012, **22**, 20535–20541.

22 J. Kim, H. Kim and S. Lee, *Chem. Mater.*, 2017, **29**, 3363–3366.

23 W. Deriouche, E. Anger, M. Freire, A. Maignan, N. Amdouni and V. Pralong, *Solid State Sci.*, 2017, **72**, 124–129.

24 Z. Jian, W. Han, X. Lu, H. Yang, Y. S. Hu, J. Zhou, Z. Zhou, J. Li, W. Chen, D. Chen and L. Chen, *Adv. Energy Mater.*, 2013, **3**, 156–160.

25 Y. H. Jung, C. H. Lim and D. K. Kim, *J. Mater. Chem. A*, 2013, **1**, 11350–11354.

26 G. Kresse and J. Hafner, *Phys. Rev. B*, 1993, **47**, 558–561.

27 G. Kresse and J. Hafner, *Phys. Rev. B*, 1994, **49**, 14251–14269.

28 G. Kresse and J. Furthmüller, *Comput. Mater. Sci.*, 1996, **6**, 15–50.

29 G. Kresse and J. Furthmüller, *Phys. Rev. B*, 1996, **54**, 11169–11186.

30 P. E. Blöchl, *Phys. Rev. B*, 1994, **50**, 17953–17979.

31 G. Kresse and D. Joubert, *Phys. Rev. B*, 1999, **59**, 1758–1775.

32 J. P. Perdew, A. Ruzsinszky, G. I. Csonka, O. A. Vydrov, G. E. Scuseria, L. A. Constantin, X. Zhou and K. Burke, *Phys. Rev. Lett.*, 2008, **100**, 136406.

33 A. A. Tsirlin, R. Nath, A. M. Abakumov, Y. Furukawa, D. C. Johnston, M. Hemmida, H.-A. Krug von Nidda, A. Loidl, C. Geibel and H. Rosner, *Phys. Rev. B*, 2011, **84**, 14429.

34 J. Heath, H. Chen and M. S. Islam, *J. Mater. Chem. A*, 2017, **5**, 13161–13167.

35 S. Grimme, J. Antony, S. Ehrlich and H. Krieg, *J. Chem. Phys.*, 2010, **132**, 154104.

36 C. Eames, J. M. Clark, G. Rousse, J. M. Tarascon and M. S. Islam, *Chem. Mater.*, 2014, **26**, 3672–3678.

37 M. S. Islam and C. A. J. Fisher, *Chem. Soc. Rev.*, 2014, **43**, 185–204.

38 J. M. Clark, C. Eames, M. Reynaud, G. Rousse, J.-N. Chotard, J.-M. Tarascon and M. S. Islam, *J. Mater. Chem. A*, 2014, **2**, 7446–7453.

39 J. Roos, C. Eames, S. M. Wood, A. Whiteside and M. S. Islam, *Phys. Chem. Chem. Phys.*, 2015, **17**, 22259–22265.

40 C. Tealdi, J. Heath and M. S. Islam, *J. Mater. Chem. A*, 2016, **4**, 6998–7004.

41 LAMMPS website, http://lammps.sandia.gov.

42 S. Plimpton, *J. Comput. Phys.*, 1995, **117**, 1–19.

43 R. V. Panin, R. V. Shpanchenko, A. V. Mironov, Y. A. Velikodny, E. V. Antipov, V. A. Tarnopolsky, A. B. Yaroslavtsev, E. E. Kaul, C. Geibel and J. Hadermann, *Chem. Mater.*, 2004, **16**, 1048–1055.

44 M. Ren, Z. Zhou, Y. Li, X. P. Gao and J. Yan, *J. Power Sources*, 2006, **162**, 1357–1362.

45 Q. Kuang, Y. Zhao, X. An, J. Liu, Y. Dong and L. Chen, *Electrochim. Acta*, 2010, **55**,

1575–1581.

46 C. Deng, S. Zhang, S. Y. Yang, Y. Gao, B. Wu, L. Ma, B. L. Fu, Q. Wu and F. L. Liu, *J. Phys. Chem. C*, 2011, **115**, 15048–15056.
Ignatov and J. B. Goodenough, *J. Electrochem. Soc.*, 2012, **159**, A1573–A1578.

47 Y. Zhang, Q. Huo, Y. Lv, L. Wang, A. Zhang, Y. Song, G. Li, H. Gao, T. Xia and H. Dong, *J. Alloys Compd.*, 2012, **542**, 187–191.

48 L.-L. Zhang, G. Liang, G. Peng, Y.-H. Huang, L. Wang, L. Qie, M. C. Croft, A.

49 D. Tao, S. Wang, Y. Liu, Y. Dai, J. Yu and X. Lei, *Ionics (Kiel).*, 2015, **21**, 1201–1239.

50 C. Lai, Z. Chen, H. Zhou, Y. Lu and H. Li, *J. Mater. Sci.*, 2015, **50**, 3075–3082.

51 H.-B. Sun, L.-L. Zhang, X.-L. Yang, G. Liang and Z. Li, *Dalt. Trans.*, 2016, **45**, 15317–15325.

52 B. Zhang, H. Chen, H. Tong, X. Wang, J. Zheng, W. Yu, J. Zhang, J. Li and W. Zhang, *J. Alloys Compd.*, 2017, **728**, 976–983.

53 A. Ponrouch, R. Dedryvère, D. Monti, A. E. Demet, J. M. Ateba Mba, L. Croguennec, C. Masquelier, P. Johansson and M. R. Palacín, *Energy Environ. Sci.*, 2013, **6**, 2361–2369.

54 W. Sun and J. Du, *Comput. Mater. Sci.*, 2017, **126**, 326–335.

55 M. J. Aragón, P. Lavela, R. Alcántara and J. L. Tirado, *Electrochim. Acta*, 2015, **180**, 824–830.

56 X. Zhao, G. Liang, H. Liu and Y. Liu, *RSC Adv.*, 2018, **8**, 4142–4152.

57 D. Jin, H. Qiu, F. Du, Y. Wei and X. Meng, *Solid State Sci.*, 2019, **93**, 62–69.

58 L. Zhao, H. Zhao, Z. Du, N. Chen, X. Chang, Z. Zhang, F. Gao, A. Trenczek-Zajac and K. Świerczek, *Electrochim. Acta*, 2018, **282**, 510–519.

59 P. A. Aparicio, J. A. Dawson, M. S. Islam and N. H. de Leeuw, *J. Phys. Chem. C*, 2018, **122**, 25829–25836.

60 T. Shibata, W. Kobayashi and Y. Moritomo, *Appl. Phys. Express*, 2013, **6**, 97101.

61 T. Shibata, W. Kobayashi and Y. Moritomo, *Appl. Phys. Express*, 2014, **7**, 67101.

59B

62 J. C. Treacher, S. M. Wood, M. S. Islam and E. Kendrick, *Phys. Chem. Chem. Phys.*, 2016, **18**, 32744–32752.

High 3D Na-ion diffusion

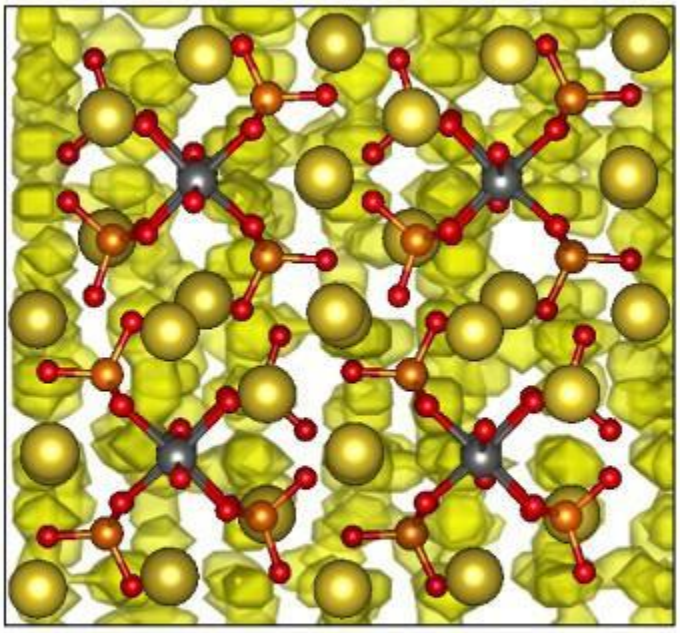

Na V P O